RSC Advances

PAPER

View Article Online
View Journal | View Issue

Cite this: *RSC Adv.*, 2022, **12**, 21332

Synthesis and bioimaging of a BODIPY-based fluorescence quenching probe for Fe^{3+}†

Junqiang Leng, Xinyu Lan, Shuang Liu, Wenxuan Jia, Wenshuai Cheng, Jianbo Cheng and Zhenbo Liu *

Iron is the main substance for maintaining life. Real-time determination of ferric ion (Fe^{3+}) in living cells is of great significance for understanding the relationship of Fe^{3+} concentration changes with various physiological and pathological processes. Fluorescent probes are suitable for the detection of trace metal ions in cells due to their low toxicity and high sensitivity. In this work, a boron-dipyrromethene-based fluorescent probe (**BODIPY-CL**) for selective detection of Fe^{3+} was synthesized. The fluorescence emission of **BODIPY-CL** was determined at 516 nm. In a pH range of 1 to 10, the probe **BODIPY-CL** exhibits a quenching response to Fe^{3+}. Meanwhile, **BODIPY-CL** showed a highly selective response to Fe^{3+} compared with 16 kinds of metal ions. The stoichiometry ratio of **BODIPY-CL** bound to Fe^{3+} was nearly 2 : 1. The fluorescence quenching response obtained by the sensor was linear with the Fe^{3+} concentration in the range of 0–400 μM, and the detection limit was 2.9 μM. **BODIPY-CL** was successfully applied to image Fe^{3+} in cells. This study provides a promising fluorescent imaging probe for further research on the physiological and pathological effects of Fe^{3+}.

Received 8th February 2022
Accepted 18th May 2022

DOI: 10.1039/d2ra00818a

rsc.li/rsc-advances

1. Introduction

Iron is essential to many physiological processes in living systems,[1] including oxygen transport,[2] energy metabolism,[3] synthesis of vitamins and steroid hormones,[4] metabolism of drugs and exogenous substances,[5] nucleotide synthesis and cell growth.[6] However, abnormal iron concentrations can cause severe diseases, such as abdominal pain and Alzheimer's and Parkinson's disease, in humans.[7,8] In addition, high levels of Fe^{3+} in algal cells can lead to variations in their morphology.[9] The specific mechanism of Fe^{3+} participating in life activities in organisms is not clear. Therefore, it is of great significance to accurately determine the concentration of Fe^{3+} in living cells.

For monitoring metal ions in living cellular organisms, fluorescent probes, with the advantages of sensitivity, simplicity, high selectivity and real-time monitoring, are an effective tool. Fluorescent probes have been widely used in the detection of trace iron ions[10–19] and the imaging of Fe^{3+} in living cells, which provides a powerful means to study the role of Fe^{3+} in life activities.[20]

For fluorescent probes, in order to better recognize Fe^{3+}, the design of recognition groups is the key.[21–24] Previously reported[25–30] probes used to detect Fe^{3+} mainly have two recognition modes. The first mode is the probe design based on the participation of Fe^{3+} in many oxidation and hydrolysis reactions, including oxidation of catechol,[31] ferrocene,[32] hydroxylamine[33] and hydrolysis of acetal,[34] Schiff base,[35] and chelation of Fe^{3+} with fluorophores.[36] And the other mode is the probe chelated with iron ions, which mostly introduce groups containing N, S and O elements into the probe. The chelation of iron ions with the introduced elements can cause changes in fluorescence properties and detect iron ions.[37–39] While, can the introduction of other heteroatoms into probe molecules also interact with iron ions to cause fluorescence changes?

As for the composition of fluorescent probes, coumarin,[40–42] rhodamine,[43–45] cyanine,[46–48] boron-dipyrromethene (BODIPY)[49–51] and 1,8-naphthalimide[52,53] are the most common fluorophores. Among them, BODIPY have the characteristics of high fluorescence quantum yield and excellent optical stability.[54–57] In addition, its chemical stability, insensitivity to the polarity and pH, and low cytotoxicity make it ideal for in bioimaging.[58–60]

Recently, we found that the introduction of *p*-phenylmethyl chloride on the BODIPY fluorophore can react with Fe^{3+}, resulting in a change in fluorescence properties. Taking advantage of this, we synthesized a fluorescent probe not been reported and established a method for Fe^{3+} detection. This work may provide a new strategy for the determination of iron ions.

2. Experimental

2.1 Reagents and instrumentation

All reagents were analytical pure and were used directly without further purification. The salts of $FeCl_3 \cdot 6H_2O$, NaCl, KCl, LiCl,

School of Chemistry and Chemical Engineering, Yantai University, Yantai 264005, P. R. China. E-mail: zhenboliu@foxmail.com

† Electronic supplementary information (ESI) available: Additional supporting information may be found in the online version of the publisher's website. See https://doi.org/10.1039/d2ra00818a

$MgCl_2 \cdot 6H_2O$, $AlCl_3 \cdot 9H_2O$, $BaCl_2 \cdot 2H_2O$, $CaCl_2$, $ZnCl_2$, $HgCl_2$, $CdCl_2$, $NiCl_2 \cdot 6H_2O$, $CoCl_2 \cdot 6H_2O$, $CrCl_3 \cdot 6H_2O$, $CuCl_2 \cdot 2H_2O$, and $Pb(NO_3)_2$ were dissolved in ultra-pure water, respectively, to prepare the concentration of 100.0 mM solution. The fluorescent probe **BODIPY-CL** was dissolved in CH_3CN to prepare the stock solution with a concentration of 1.0 mM. The stock solution was further diluted in buffers to obtain working solutions. All buffers were phosphate-buffered saline solution (PBS, pH = 7.4) containing CH_3CN, (PBS/CH_3CN = 8 : 2, v/v). The column chromatography used 200–300 mesh silica gel (Qingdao Haiyang Chemical Co., China). Thin-layer chromatography (TLC) was performed on silica gel 60 F_{254} plates (20 cm × 20 cm, 0.25 mm thickness) (Merck, Germany). The ^1H and ^{13}C nuclear magnetic resonance (NMR) absorption spectra were measured by using a 400 MHz Bruker spectrometer. The ultra-violet (UV) spectrum was measured with PerkinElmer LAMBDA 365 spectrophotometer using a quartz cuvette with a path length of 1.0 cm. Fluorescence spectra were recorded by Varian Cary Eclipse fluorescence spectrophotometer using 1 cm quartz cuvette with excitation wavelength of 371 nm and temperature of 25 °C. Cell images were taken with a fluorescence microscope (Olympus, IX73). The wavelength of the filter is 505 nm. The pH value was measured using a pH meter (Ohaus, ST3100).

2.2 Synthesis of BODIPY-CL

The synthesis procedure was modified according to the procedure described in the literature.[61] 0.95 g (10 mmol) of 2,4-dimethylpyrrole was added to 100 mL of dichloromethane solution containing 4-chloromethylbenzaldehyde (0.77 g, 5 mmol). The solution was stirred under N_2 atmosphere at room temperature for 12 h. Add triethylamine (10 mL) and stir for 1 h. Thereafter, 1.14 g (5 mmol) of 2,3-dichloro-5,6-dicyano-1,4-benzoquinone (DDQ) and 10 mL of boron trifluoride ether complex were added and stirred for 3 h. Then the crude product obtained by removing the solvent through rotary evaporator was purified by column chromatography with petroleum ether/ethyl acetate (1/3) as eluent to obtain orange solid **BODIPY-CL** (0.43 g, 23.4%). ^1H NMR (400 MHz, $CDCl_3$) δ: 7.58–7.51 (m, 2H), 7.35–7.29 (m, 2H), 6.01 (s, 2H), 4.68 (s, 2H), 2.58 (s, 6H), and 1.40 (s, 6H); ^{13}C NMR (101 MHz, DMSO-d_6) δ: 155.46, 143.15, 141.92, 139.45, 134.38, 131.07, 130.13, 128.64, 121.93, 46.01, 14.69, and 14.50. HRMS (EI): calcd for $C_{20}H_{20}BClF_2N_2$ $[M + Na]^+$: 395.1346, found: 395.1271.

2.3 Limit of detection (LOD)

To calculate the standard deviation (σ) of blank solution, the fluorescence intensity of **BODIPY-CL** without Fe^{3+} was determined 11 times. The emission intensity of probe at 516 nm was measured with the increase of Fe^{3+} concentration. And the slope (k) of the curve that the emission intensity decreases with the increase of Fe^{3+} concentration was obtained (Fig. 2d). The LOD was based on $3\sigma/k$ according to the literature report.[62]

2.4 Computational details

Using density functional theory (DFT), the optimized structure of **BODIPY-CL** was obtained at B3LYP/6-31+G(d,p) level.[63] The HOMO and LUMO energies of **BODIPY-CL** were calculated. The absorption spectrum was computed by time-dependent (TD)-DFT using B3LYP functional with the 6-31+G(d,p) basis set. The calculations were all conducted with GAUSSIAN 09 program package.[64]

2.5 Cytotoxicity assays

HeLa cells were purchased from Shanghai iCell Bioscience Inc. (Shanghai, China). Cells (4×10^3 cells per well) were seeded into 96-well plates in a 37 °C, 5% CO_2 incubator for 24 h. Next, the probe **BODIPY-CL** at four concentrations (3.125 μM, 6.25 μM, 12.5 μM or 25.0 μM) was added and incubated for 12 h. After that, 0.5 mg mL^{-1} of 3-(4,5-dimethylthiazol-2-yl)-2,5-diphenyltetrazolium bromide (MTT) solution was added. After 4 h, remove medium carefully, and add 100.0 μL of dimethyl sulphoxide (DMSO) to the wells with the purpose of dissolving formazan crystals. Afterward, the absorbance was measured at 570 nm.

2.6 Fluorescence imaging

HeLa cells were cultured in Dulbecco's Modified Eagle's Medium containing 10% fetal bovine serum (FBS) in 24-well plates at 37 °C with 5% CO_2 for 24 h. Then probe **BODIPY-CL** dissolved in DMSO at a concentration of 10 μM was added to the cells. After 30 min, fluorescence imaging was carried out using a fluorescence microscope with a 100× objective lens. Then, add 50 μM Fe^{3+} solution and incubate for 30 min. Before each step, the cells were rinsed with PBS three times. White light and fluorescence images were then obtained using the methods described previously.

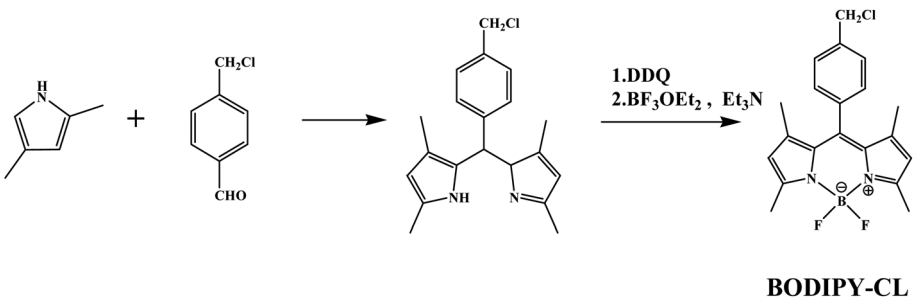

BODIPY-CL

Scheme 1 Synthesis of the BODIPY-CL fluorescent probe.

3. Results and discussion

3.1 Design of probe BODIPY-CL

In this paper, using BODIPY as fluorophore, we synthesized a fluorescent probe (**BODIPY-CL**) for the determination of ferric ion (Fe^{3+}). The BODIPY derivative with one *p*-chloromethylbenzene unit can be complexed with ferric ion (Fe^{3+}) to cause fluorescence quenching. Scheme 1 showed the synthetic route for **BODIPY-CL**. Details of the experimental procedure and

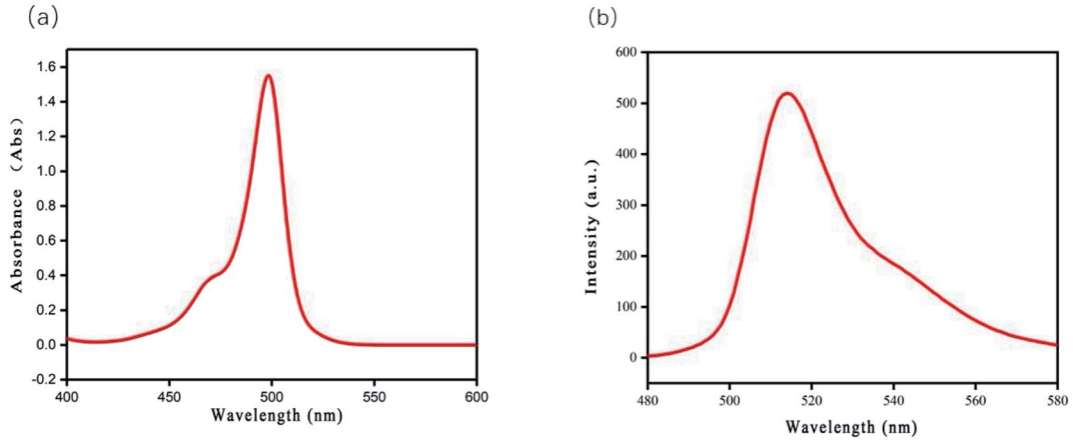

Fig. 1 (a) UV-vis absorbance spectra and (b) fluorescence emission spectra (λ_{ex} = 371 nm) of **BODIPY-CL** (10 μM) in PBS/acetonitrile (8 : 2, v/v, pH = 7.4) buffer solution.

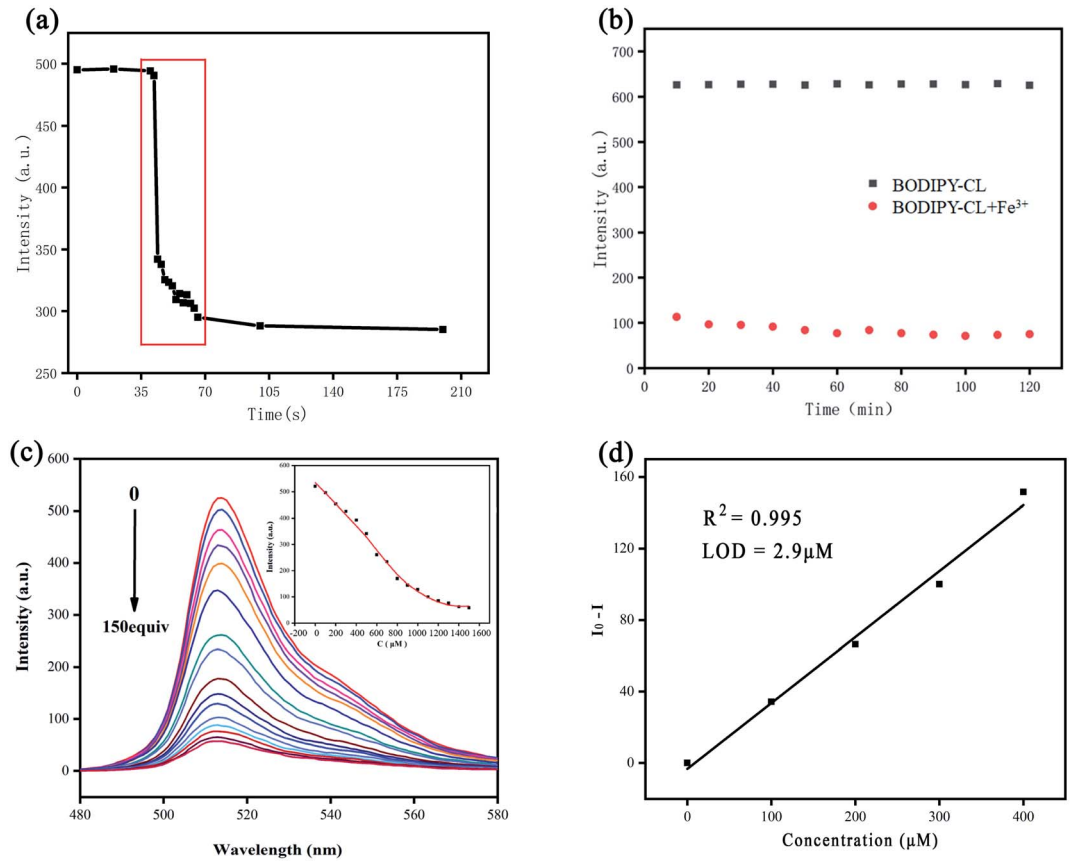

Fig. 2 (a) Emission intensity at 512 nm of **BODIPY-CL** (10 μM) with Fe^{3+} (1 mM) as a function of the time under PBS/acetonitrile (8 : 2, v/v, pH = 7.4) buffer solution. (λ_{ex} = 371 nm); (b) emission intensity at 512 nm of **BODIPY-CL** (10 μM) with Fe^{3+} (1 mM) under PBS/acetonitrile (8 : 2, v/v, pH = 7.4) buffer solution. (λ_{ex} = 371 nm); (c) fluorescence emission spectra (λ_{ex} = 371 nm) of **BODIPY-CL** (10 μM) in PBS/acetonitrile (8 : 2, v/v, pH = 7.4) buffer solution with various concentrations of Fe^{3+} (0–1500.0 μM). The inset shows the fluorescence intensity at 512 nm *versus* Fe^{3+} concentration. Each datum was acquired 10 min after Fe^{3+} was added; (d) reduction of emission intensity at 512 nm of **BODIPY-CL** (10 μM) change as a function of Fe^{3+} (at 0–400 μM) under PBS/acetonitrile (8 : 2, v/v, pH = 7.4) buffer solution. (λ_{ex} = 371 nm).

Table 1 Comparison of fluorescent probes for Fe^{3+}

Probes	Detection limit (nM)	Response time (s)	Ref.
BODIPY-CL	2900	20	This work
PY4	140	—	65
P2	1240	<60	66
Cell-BODIPY	1720	600	67
BODIPY-NIR	14.2	1800	68
BODIPY-PH	580	1800	69

characteristics of **BODIPY-CL** can be found in the Experimental section and ESI (Fig. S1–S3†).

3.2 Fluorescence and UV-vis response of BODIPY-CL to Fe^{3+}

UV-vis and fluorescence spectra of **BODIPY-CL** were determined in CH_3CN/PBS buffer (v/v = 2 : 8). Fig. 1 displays the typical optical properties of the BODIPY chromophore, with a maximum absorption wavelength of 498 nm (Fig. 1a) and a maximum emission wavelength of 516 nm (Fig. 1b). Response times of **BODIPY-CL** to Fe^{3+} were also evaluated using fluorescence spectra (see Fig. 2a). The magneton was placed in a quartz cuvette containing the probe solution to achieve the mixing of the probe solution and the iron ion solution. The emission intensity at 516 nm decreases drastically within less than 20 s after Fe^{3+} was added. The response time of **BODIPY-CL** for Fe^{3+} detection was quite fast.

The stability of fluorescence intensity was also investigated. Fig. 2b shows the changes of fluorescence intensity over time with or without the addition of Fe^{3+} in **BODIPY-CL** solution under continuous UV irradiation. The **BODIPY-CL** probe exhibited a stable fluorescence emission intensity under UV light irradiation for 2 h in the absence of Fe^{3+}, suggesting the high photochemical stability of the prob. While, when Fe^{3+} was added to **BODIPY-CL** solution, the fluorescence emission at 516 nm decreased and the luminescence property was also stable. The quenching efficiency was calculated according to the equation: $[1 - (F/F_0)] \times 100\%$. The relationship of **BODIPY-CL** fluorescence intensity to Fe^{3+} addition concentration was investigated (in Fig. 2c). The intensity decreases with the increase of Fe^{3+} concentration. Meanwhile, the intensity shows a negative linear relationship with the Fe^{3+} concentration in the range of 0 to 400.0 μM. And the linear correlation coefficient (R^2) was 0.995 (Fig. 2d). The limits of detection (LOD) of the method was also calculated as 2.9 μM. The detection limit and response time of **BODIPY-CL** are tabulated and compared with previous literature (Table 1).[65–69]

3.3 Selectivity study

In order to evaluate the selectivity, the emission intensity of the **BODIPY-CL**, **BODIPY-CL** with Fe^{3+} and **BODIPY-CL** with the addition of others metal ions (Na^+, K^+, Li^+, Mg^{2+}, Al^{3+}, Ba^{2+}, Ca^{2+}, Zn^{2+}, Hg^{2+}, Cd^{2+}, Ni^{2+}, Co^{2+}, Cr^{2+}, Cu^{2+} and Pb^{2+}) was measured (see Fig. 3a and b). The colorimetric and fluorescence changes

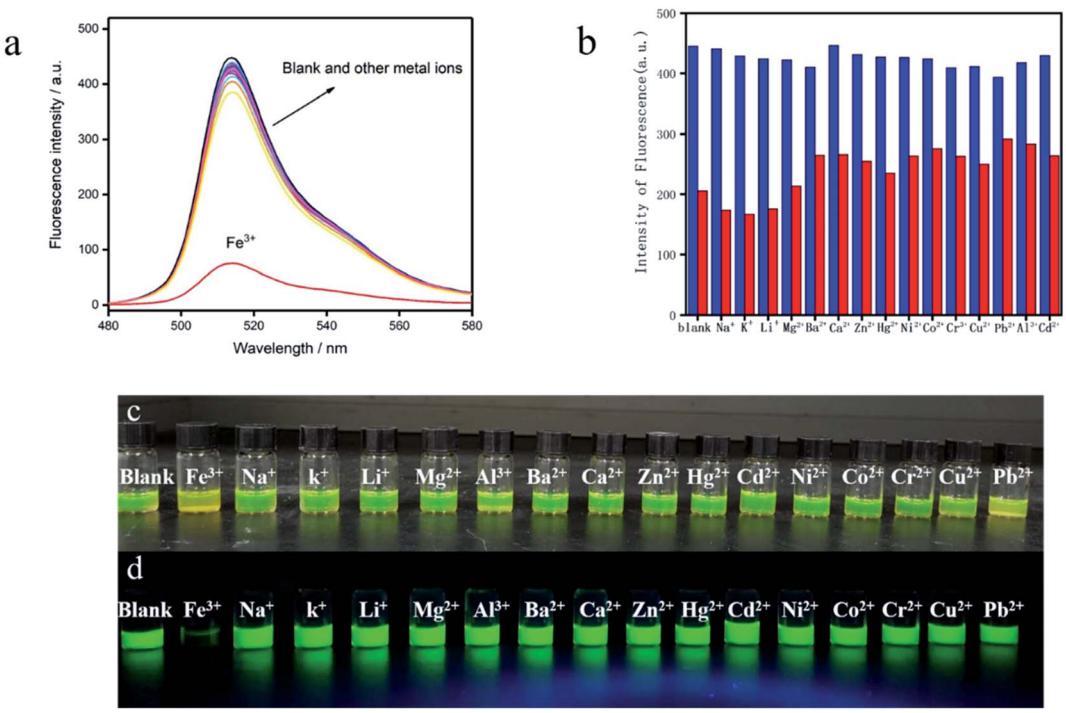

Fig. 3 (a) Fluorescence changes in **BODIPY-CL** (10 μM) mixed with 100 equiv. of Fe^{3+} and other metal ions (Na^+, K^+, Li^+, Mg^{2+}, Al^{3+}, Ba^{2+}, Ca^{2+}, Zn^{2+}, Hg^{2+}, Cd^{2+}, Ni^{2+}, Co^{2+}, Cr^{2+}, Cu^{2+} and Pb^{2+}) in PBS/acetonitrile (8 : 2, v/v, pH = 7.4) buffer solution. λ_{ex} = 371 nm; (b) emission intensity (512 nm) of **BODIPY-CL** (10 μM) mixed with Fe^{3+} (100 equiv.) and other metal ions (100 equiv.) in PBS/acetonitrile (8 : 2, v/v, pH = 7.4) buffer solution. λ_{ex} = 371 nm; (c) color change in **BODIPY-CL** (100 μM) upon the addition of various metal ions (50 equiv.) under ambient light; (d) visible emission color images of **BODIPY-CL** (100 μM) upon the addition of various metal ions (50 equiv.) under UV irradiation by a UV lamp. λ = 365 nm.

of **BODIPY-CL** for Fe^{3+} and 16 metal ions are observed by naked eyes. Only with the addition of Fe^{3+} and Pb^{2+} ions, the color of **BODIPY-CL** probe solution changed from yellow-green to light yellow. While, the addition of other metal ions does not change the color of the solution (Fig. 3c). Interesting, the fluorescence response immediately weakens and almost completely disappears with the addition of Fe^{3+} ion (Fig. 3d) under the UV-light irradiation (λ = 365 nm). In contrast, when other metal ions, including Pb^{2+} ion, were added to the probe solution, the luminescence intensity did not change obviously. According to the above results, Fe^{3+} and Pb^{2+} ions can interact with the probe molecules. While, the other ions do not interact with the probe. At the same time, only the interaction of Fe^{3+} ion can cause fluorescence quenching of **BODIPY-CL** probe. It is indicated that the probe has good fluorescence quenching selectivity for Fe^{3+}.

3.4 Effect of co-existing metal ions on Fe^{3+} detection

The **BODIPY-CL** probe was incubated with other ions (Na^{+}, K^{+}, Li^{+}, Mg^{2+}, Ba^{2+}, Ca^{2+}, Zn^{2+}, Hg^{2+}, Ni^{2+}, Co^{2+}, Cr^{3+}, Cu^{2+}, Pb^{2+}, Al^{3+}, and Cd^{2+}) in buffer, and the fluorescence intensity was detected. As mentioned above, the fluorescence intensity changes little in the presence of other ions compared to the absence of ions (blue columns in Fig. 3b). Then, Fe^{3+} was added to the above solution with the probe and co-existing metal ion, the fluorescence emission intensity is obviously reduced (see the red columns in Fig. 3b). In general, the quenching response of **BODIPY-CL** to Fe^{3+} is not affected by most other metal ions.

3.5 Effect of pH

The capability of **BODIPY-CL** to detect Fe^{3+} in various pH buffer solutions was investigated in detail (Fig. S4†). In the pH range of 1.0 to 10.0, the recognition ability of **BODIPY-CL** to Fe^{3+} is nearly invariant. It is indicated that the probe may determine Fe^{3+} ion in a wide range of pH values, expanding the probe's ability to detect Fe^{3+} ion in cells.

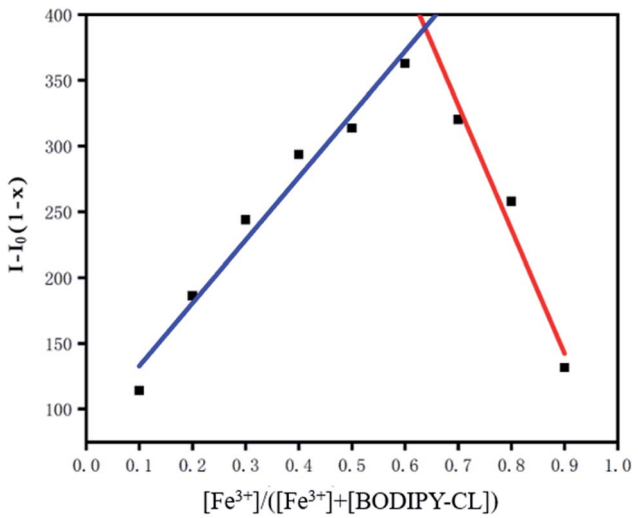

Fig. 4 Job's plot for **BODIPY-CL** titrated with Fe^{3+} indicating the formation of 1 : 1 complexes. The total [Fe^{3+}] + [**BODIPY-CL**] = 1 × 10−4 M. (x = [Fe^{3+}]/[Fe^{3+}] + [**BODIPY-CL**]).

3.6 Binding mode study

In order to investigate whether REDOX reaction occurred between the probe and iron ion, *o*-phenanthroline was added into the mixed solution of probe and iron ion. There was no significant discoloration in the solution, indicating that no Fe^{2+} ions were formed and the REDOX reaction did not occur.

The binding stoichiometric ratio of **BODIPY-CL** to Fe^{3+} was investigated by fluorescence titration experiments.[70] The total concentration of the **BODIPY-CL** and Fe^{3+} was fixed at 10^{-4} M. The Job's plot in Fig. 4 showed that the maximum relative intensity appears at [Fe^{3+}]/([Fe^{3+}] + [**BODIPY-CL**]) = 0.66, which shows that **BODIPY-CL** and Fe^{3+} form a complex with a molar ratio of 1 : 2.[71]

Additionally, the probe forms the 1 : 2 complex with ferric ion, which was also confirmed by the positive ion mode mass

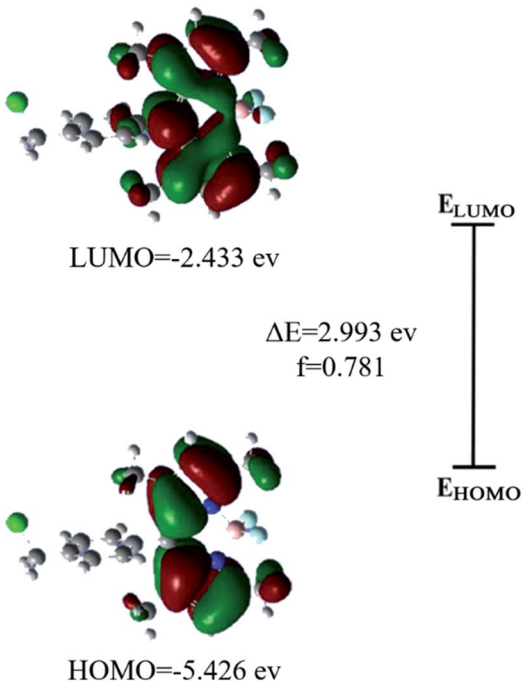

Fig. 5 Frontier molecular orbital diagram depicting the HOMO and LUMO of the **BODIPY-CL** probe.

Table 2 The testing results of Fe^{3+} concentration in tap water samples (n = 3)

Water samples	Fe^{3+} spiked (μM)	Found mean (μM)	Recovery (%)
Tap water 1	0.0	ND[a]	—
Tap water 2	10.0	10.4	104.0
Tap water 3	20.0	17.9	89.5
Tap water 4	30.0	30.5	101.7

[a] None detected.

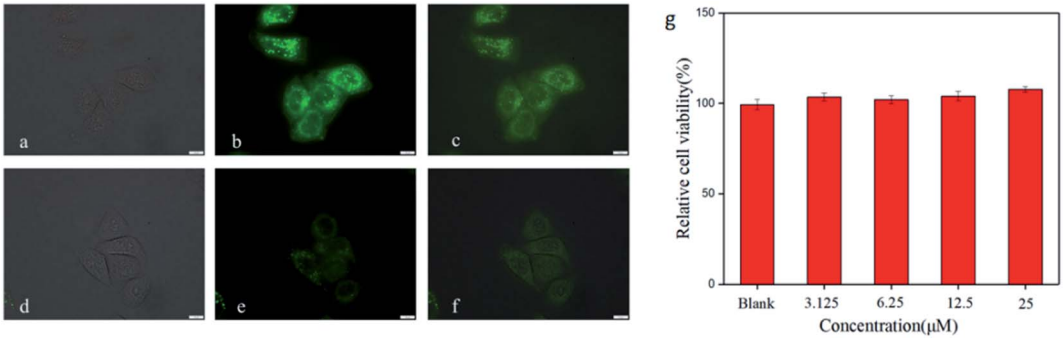

Fig. 6 Images of HeLa cells treated with the **BODIPY-CL** probe: (a) bright field image of HeLa cells incubated with **BODIPY-CL** (25 μM); (b) green channel fluorescence image of (a); (c) overlay image of (a) and (b); (d) bright field image of HeLa cells incubated with **BODIPY-CL** (25 μM) for 30 min followed by incubation with Fe^{3+} (250 μM) for 30 min at 37 °C; (e) green channel fluorescence image of (d); (f) overlay image of (d) and (e). λ_{ex} = 460 nm; (g) cytotoxicity assays of **BODIPY-CL** at different concentrations for HeLa cells.

spectrometry data of electrospray ionization mass spectrometry (ESI-MS). A peak in ESI-MS at m/z = 481.29 (Fig. S5†) exactly corresponds to [**BODIPY-CL** + $2Fe^{3+}$]$^+$ (the complexation of **BODIPY-CL** with two Fe^{3+} ions loss of four hydrogen ions).

3.7 Theoretical calculations

To better understand the photophysical properties of chemosensors, theoretical computational methods are often used.[72] Optimized structures (in Fig. S6†) of **BODIPY-CL** were obtained by using DFT calculations. Energies of relevant orbitals of the **BODIPY-CL** were listed in Table S1.† According to the frontier orbital analysis, the distribution of electrons in HOMO and LUMO orbitals shows that electrons are localized on the BODIPY group during the transition (see Fig. 5). Through time density functional theory studies, it is found that the electronic transition at the maximum absorption wavelength occurs in the HOMO–LUMO transition. Thus, the **BODIPY-CL** probe exhibited strong fluorescent behavior. Meanwhile, the absorption spectra (λ_{max} = 422 nm) and emission spectra (λ_{max} = 484 nm) of the **BODIPY-CL** chemosensor obtained by DFT theoretical calculation were in Fig. S7 and S8.† The experimental results were red-shifted compared with the theoretical calculations, which may be due to the influence of the solvent, because the solvent in the actual detection was a mixed solution of ethanol and PBS.

3.8 Detection of Fe^{3+} in water samples

To further evaluate the feasibility of **BODIPY-CL** for rapid and sensitive detection of Fe^{3+} in practical applications, tap water was detected by fluorescence spectroscopy. Detection results are collected in Table 2. No Fe^{3+} was detected in tap water. The spiked experiment showed good recovery rates, which were between 89.5% and 104.0%. It can be seen that the probe is accurate and reliable in detecting Fe^{3+} in environmental samples.

3.9 Live-cell imaging

Fluorescence imaging of living HeLa cells was shown in Fig. 6. A strong green fluorescence signal in the cell was observed (Fig. 6b) when cells were incubated with **BODIPY-CL**. However, the fluorescence intensity of **BODIPY-CL** probe loaded cells decreased after Fe^{3+} was added (see Fig. 6e). In addition, *in vitro* cytotoxicity studies were performed using HeLa cells, and the results were shown in Fig. 6g that the **BODIPY-CL** probe has almost no toxicity to living cells under fluorescence cell imaging conditions. Therefore, the **BODIPY-CL** can penetrate the cell membrane and be used in response to Fe^{3+} in living cells.

4. Conclusions

A fluorescent probe **BODIPY-CL** was synthesized and applied to detect Fe^{3+}. Based on the quenching effect of Fe^{3+} on the probe, a method to detect Fe^{3+} was developed. The probe shows highly sensitive and selective response to Fe^{3+}. The fluorescence quenching response is linear with the Fe^{3+} concentration over the range of 0 to 400 μM, and the detection limit is 2.9 μM. The stoichiometric ratio of **BODIPY-CL** to Fe^{3+} is nearly 2 : 1. **BODIPY-CL** was successfully applied to imaging Fe^{3+} in cells, which is helpful to provide a promising fluorescent imaging probe for further research on the physiological and pathological effects of Fe^{3+}.

Conflicts of interest

This research work is not funded by any organization and has no potential conflict of interest.

Acknowledgements

This work was supported by the National Natural Science Foundation of China (No. 21705139) and Innovative Training Program for College Students in Shandong Province (No. S202011066025).

References

1 H. Wang, D.-L. Shi, J. Li, H.-Y. Tang, J. Li and Y. Guo, *Sens. Actuators, B*, 2018, **256**, 600–608.

2 M. T. Wilson and B. J. Reeder, *Exp. Physiol.*, 2008, **93**, 128–132.
3 A. S. Grillo, A. M. SantaMaria, M. D. Kafina, A. G. Cioffi, N. C. Huston, M. Han, Y. A. Seo, Y. Y. Yien, C. Nardone, A. V. Menon, J. Fan, D. C. Svoboda, J. B. Anderson, J. D. Hong, B. G. Nicolau, K. Subedi, A. A. Gewirth, M. Wessling-Resnick, J. Kim, B. H. Paw and M. D. Burke, *Science*, 2017, **356**, 608.
4 W. L. Miller and H. S. Bose, *J. Lipid Res.*, 2011, **52**, 2111–2135.
5 I. A. Pikuleva and M. R. Waterman, *J. Biol. Chem.*, 2013, **288**, 17091–17098.
6 W. Sornjai, F. Nguyen Van Long, N. Pion, A. Pasquer, J.-C. Saurin, V. Marcel, J. J. Diaz, H. C. Mertani and D. R. Smith, *Chem.-Biol. Interact.*, 2020, **319**, 109021.
7 L. Guo, Y. Liu, R. Kong, G. Chen, Z. Liu, F. Qu, L. Xia and W. Tan, *Anal. Chem.*, 2019, **91**, 12453–12460.
8 Y. Wu, S. Zhang, X. Gong, S. Tam, D. Xiao, S. Liu and Y. Tao, *Mol. Cancer*, 2020, **19**, 39.
9 Y. Sun, N. Zhang, Q. L. Guan, C. H. Liu, B. Li, K. Y. Zhang, G. H. Li, Y. H. Xing, F. Y. Bai and L. X. Sun, *Cryst. Growth Des.*, 2019, **19**, 7217–7229.
10 T. Hirayama, M. Niwa, S. Hirosawa and H. Nagasawa, *ACS Sens.*, 2020, **5**, 2950–2958.
11 X. Zhu, Y. Duan, P. Li, H. Fan, T. Han and X. Huang, *Anal. Methods*, 2019, **11**, 642–647.
12 T. Hirayama, M. Inden, H. Tsuboi, M. Niwa, Y. Uchida, Y. Naka, I. Hozumi and H. Nagasawa, *Chem. Sci.*, 2019, **10**, 1514–1521.
13 X.-Q. Yi, Y.-F. He, Y.-S. Cao, W.-X. Shen and Y.-Y. Lv, *ACS Sens.*, 2019, **4**, 856–864.
14 Z. Li, Y. Xu, H. Xu, M. Cui, T. Liu, X. Ren, J. Sun, D. Deng, Y. Gu and P. Wang, *Spectrochim. Acta, Part A*, 2021, **244**, 118819.
15 Y. Wang, C. Xia, Z. Han, Y. Jiao, X. Yao, Z. Lun, S. Fu, H. Zhang, P. Hou and D. Ning, *J. Photochem. Photobiol., B*, 2019, **199**, 111602.
16 Z.-H. Fu, J.-C. Qin, Y.-W. Wang, Y. Peng, Y.-M. Zhang, D.-M. Zhao and Z.-H. Zhang, *Dyes Pigm.*, 2021, **185**, 108896.
17 X. Yuan, T.-H. Leng, Z.-Q. Guo, C.-Y. Wang, J.-Z. Li, W.-W. Yang and W.-H. Zhu, *Dyes Pigm.*, 2019, **161**, 403–410.
18 Y. Tang, Y. Huang, Y. Chen, L. Lu, C. Wang, T. Sun, M. Wang, G. Zhu, Y. Yang, L. Zhang and J. Zhu, *Spectrochim. Acta, Part A*, 2019, **218**, 359–365.
19 P. Ravichandiran, V. K. Kaliannagounder, A. P. Bella, A. Boguszewska-Czubara, M. Masłyk, C. S. Kim, C. H. Park, P. M. Johnson, B.-H. Park, M.-K. Han, A. R. Kim and D. J. Yoo, *Anal. Chem.*, 2021, **93**, 801–811.
20 W. Xuan, R. Pan, Y. Wei, Y. Cao, H. Li, F.-S. Liang, K.-J. Liu and W. Wang, *Bioconjugate Chem.*, 2016, **27**, 302–308.
21 R. Kouser, S. Zehra, R. A. Khan, A. Alsalme, F. Arjmand and S. Tabassum, *Spectrochim. Acta, Part A*, 2021, **247**, 119156.
22 M. Kumar, A. Kumar, M. S. H. Faizi, S. Kumar, M. K. Singh, S. K. Sahu, S. Kishor and R. P. John, *Sens. Actuators, B*, 2018, **260**, 888–899.
23 T. Hirayama, *Free Radical Biol. Med.*, 2019, **133**, 38–45.
24 A. T. Aron, M. O. Loehr, J. Bogena and C. J. Chang, *J. Am. Chem. Soc.*, 2016, **138**, 14338–14346.
25 C.-H. Cai, H.-L. Wang and R.-J. Man, *Spectrochim. Acta, Part A*, 2021, **255**, 119729.
26 M. I. Halawa, F. Wu, A. Nsabimana, B. Lou and G. Xu, *Sens. Actuators, B*, 2018, **257**, 980–987.
27 J. Liu, Y. Guo, B. Dong, J. Sun, J. Lyu, L. Sun, S. Hu, L. Xu, X. Bai, W. Xu, S. Mintova and H. Song, *Sens. Actuators, B*, 2020, **320**, 128361.
28 Y. Wang, S. Lao, W. Ding, Z. Zhang and S. Liu, *Sens. Actuators, B*, 2019, **284**, 186–192.
29 Z. Xie, X. Sun, J. Jiao and X. Xin, *Colloids Surf., A*, 2017, **529**, 38–44.
30 X. Zhang, Z. Gou, Y. Zuo and W. Lin, *Spectrochim. Acta, Part A*, 2020, **228**, 117679.
31 S. Kuang, X. Liao, X. Zhang, T. W. Rees, R. Guan, K. Xiong, Y. Chen, L. Ji and H. Chao, *Angew. Chem., Int. Ed.*, 2020, **59**, 3315–3321.
32 M. Karmakar, S. R. Bhatta, S. Giri and A. Thakur, *Inorg. Chem.*, 2020, **59**, 4493–4507.
33 M. Wang, Y.-M. Zhang, Q.-Y. Zhao, Z.-H. Fu and Z.-H. Zhang, *Chem. Phys.*, 2019, **527**, 110470.
34 B. K. Rani and S. A. John, *J. Photochem. Photobiol., A*, 2020, **392**, 112426.
35 Y.-K. Chiang, Y. R. Bhorge, R. D. Divate, Y.-C. Chung and Y.-P. Yen, *J. Fluoresc.*, 2016, **26**, 1699–1708.
36 A. Goel, S. Umar, P. Nag, A. Sharma, L. Kumar, Shamsuzzama, Z. Hossain, J. R. Gayen and A. Nazir, *Chem. Commun.*, 2015, **51**, 5001–5004.
37 J.-S. Lee, S. D. Warkad, P. B. Shinde, A. Kuwar and S. B. Nimse, *Arabian J. Chem.*, 2020, **13**, 8697–8707.
38 Q. Wang, D. Zheng, Q. Cao, K. Huang and D. Qin, *Spectrochim. Acta, Part A*, 2021, **261**, 120061.
39 B. Li, X. Gu, M. Wang, X. Liu and K. Xu, *Dyes Pigm.*, 2021, **194**, 109637.
40 X.-G. Chen, Y. Mei, H. Li and Q.-H. Song, *Sens. Actuators, B*, 2022, **354**, 131202.
41 B. Yin, S. Zhang, H. Chen and L. Yan, *Sens. Actuators, B*, 2021, **344**, 130225.
42 A. Grzelakowska, J. Modrzejewska, J. Kolińska, M. Szala, M. Zielonka, K. Dębowska, M. Zakłos-Szyda, A. Sikora, J. Zielonka and R. Podsiadły, *Free Radical Biol. Med.*, 2022, **179**, 34–46.
43 Y. Zhang, X.-F. Zhang, Q. Chen, X.-Q. Cao and S.-L. Shen, *Sens. Actuators, B*, 2022, **353**, 131145.
44 F. Fan, L. Zhang, F. Mu and G. Shi, *ACS Sens.*, 2021, **6**, 1400–1406.
45 T. Mukherjee, S. Kanvah, A. S. Klymchenko and M. Collot, *ACS Appl. Mater. Interfaces*, 2021, **13**, 40315–40324.
46 G. Fei, S. Ma, C. Wang, T. Chen, Y. Li, Y. Liu, B. Tang, T. D. James and G. Chen, *Coord. Chem. Rev.*, 2021, **447**, 214134.
47 Q. Cheng, Y. Tian, H. Dang, C. Teng, K. Xie, D. Yin and L. Yan, *Adv. Healthcare Mater.*, 2022, **11**, 2101697.
48 X. Wang, H. N. Chan, N. Desbois, C. P. Gros, F. Bolze, Y. Li, H. W. Li and M. S. Wong, *ACS Appl. Mater. Interfaces*, 2021, **13**, 18525–18532.
49 P. Wu, Y. Zhu, S. Liu and H. Xiong, *ACS Cent. Sci.*, 2021, **7**, 2039–2048.

50 J. M. Merkes, A. Hasenbach, F. Kiessling, S. Hermann and S. Banala, *ACS Sens.*, 2021, **6**, 4379–4388.
51 M. Priessner, P. A. Summers, B. W. Lewis, M. Sastre, L. Ying, M. K. Kuimova and R. Vilar, *Angew. Chem., Int. Ed.*, 2021, **60**, 23148–23153.
52 Z. Zhang, Q. Yuan, M. Li, B. Bao and Y. Tang, *Small*, 2021, **17**, 2104581.
53 C. Geraghty, C. Wynne and R. B. P. Elmes, *Coord. Chem. Rev.*, 2021, **437**, 213713.
54 J. Bañuelos, *Chem. Rec.*, 2016, **16**, 335–348.
55 J. M. Franke, B. K. Raliski, S. C. Boggess, D. V. Natesan, E. T. Koretsky, P. Zhang, R. U. Kulkarni, P. E. Deal and E. W. Miller, *J. Am. Chem. Soc.*, 2019, **141**, 12824–12831.
56 M. Poddar, P. Gautam, Y. Rout and R. Misra, *Dyes Pigm.*, 2017, **146**, 368–373.
57 T. Zhang, C. Ma, T. Sun and Z. Xie, *Coord. Chem. Rev.*, 2019, **390**, 76–85.
58 P. Kaur and K. Singh, *J. Mater. Chem. C*, 2019, **7**, 11361–11405.
59 P. E. Kesavan, V. Pandey, M. K. Raza, S. Mori and I. Gupta, *Bioorg. Chem.*, 2019, **91**, 103139.
60 S. M. Yuriy, V. S. Alexey, S. T. Alexander and V. R. Evgeniy, *Curr. Med. Chem.*, 2017, **24**, 2745–2772.
61 P. Guo, S. Yan, J. Hu, X. Xing, C. Wang, X. Xu, X. Qiu, W. Ma, C. Lu, X. Weng and X. Zhou, *Org. Lett.*, 2013, **15**, 3266–3269.
62 G. L. Long and J. D. Winefordner, *Anal. Chem.*, 1983, **55**, 712A–724A.
63 A. D. Becke, *J. Chem. Phys.*, 1993, **98**, 5648–5652.
64 G. W. T. M. J. Frisch, H. B. Schlegel, G. E. Scuseria, J. R. C. M. A. Robb, G. Scalmani, V. Barone, B. Mennucci, H. N. G. A. Petersson, M. Caricato, X. Li, H. P. Hratchian, J. B. A. F. Izmaylov, G. Zheng, J. L. Sonnenberg, M. Hada, K. T. M. Ehara, R. Fukuda, J. Hasegawa, M. Ishida, T. Nakajima, O. K. Y. Honda, H. Nakai, T. Vreven, J. A. Montgomery Jr, F. O. J. E. Peralta, M. Bearpark, J. J. Heyd, E. Brothers, V. N. S. K. N. Kudin, T. Keith, R. Kobayashi, J. Normand, A. R. K. Raghavachari, J. C. Burant, S. S. Iyengar, J. Tomasi, N. R. M. Cossi, J. M. Millam, M. Klene, J. E. Knox, J. B. Cross, C. A. V. Bakken, J. Jaramillo, R. Gomperts, R. E. Stratmann, A. J. A. O. Yazyev, R. Cammi, C. Pomelli, J. W. Ochterski, K. M. R. L. Martin, V. G. Zakrzewski, G. A. Voth, J. J. D. P. Salvador, S. Dapprich, A. D. Daniels, J. B. F. O. Farkas, J. V. Ortiz, J. Cioslowski and a. D. J. Fox, *Gaussian 09 programme packages was used toperform all the electronic structure calculations and visualizations*, Wallingford CT, 2010.
65 L. Xiao, C. Li, X. He and X. Cheng, *SN Appl. Sci.*, 2021, **3**, 591.
66 S. He, L. Xiao, L. Marin, Y. Bai and X. Cheng, *Eur. Polym. J.*, 2021, **150**, 110428.
67 M. Oguz, A. N. Kursunlu and M. Yilmaz, *Dyes Pigm.*, 2020, **173**, 107974.
68 J. Ji, S. S. Chereddy, Y. Ren, X. Chen, D. Su, Z. Zhong, T. Mori, Y. Inoue, W. Wu and C. Yang, *J. Photochem. Photobiol., A*, 2018, **355**, 78–83.
69 J. Nootem, C. Sattayanon, R. Daengngern, A. Kamkaew, W. Wattanathana, S. Wannapaiboon, P. Rashatasakhon and K. Chansaenpak, *Chemosensors*, 2021, **9**, 165.
70 H. Wang, D. Wang, Q. Wang, X. Li and C. A. Schalley, *Org. Biomol. Chem.*, 2010, **8**, 1017–1026.
71 L.-m. Liu and Z.-y. Yang, *Inorg. Chim. Acta*, 2018, **469**, 588–592.
72 T. Keawwangchai, N. Morakot and B. Wanno, *J. Mol. Model.*, 2013, **19**, 1435–1444.